Resonance Raman Intensity Analysis of Merocyanine Dimers in Solution†

Weinan Leng,‡ Frank Würthner,§ and Anne Myers Kelley*,‡

School of Natural Sciences, University of California, Merced, P.O. Box 2039, Merced, California 95344, and Institut für Organische Chemie, Universität Würzburg, Am Hubland, 97074 Würzburg, Germany

Received: November 5, 2003; In Final Form: December 19, 2003

Resonance Raman excitation profiles and absolute cross sections are presented for three closely related merocyanine dyes as monomers in dichloromethane solution and as H-dimers in dioxane solution. For both monomers and dimers the absorption spectra and the resonance Raman intensities of the 24 to 30 strongest vibrations are quantitatively simulated using time-dependent wave packet propagation methods to determine the geometry changes along each Franck−Condon active mode upon electronic excitation, as well as the homogeneous and inhomogeneous electronic line widths. In addition, an approach previously formulated to describe the vibronic structure of an excitonically coupled homodimer with multiple vibrational modes [Kelley, A. M. *J. Chem. Phys.* **2003**, *119*, 3320−3331] is applied to model the dimer spectra. Comparison of these two calculations demonstrates that when the intermonomer coupling is strong the theoretical absorption and resonance Raman spectra of the dimer can be very well approximated by treating the system as a "supermolecule" having a single electronic transition with appropriately rescaled vibrational displacements, transition dipole, and electronic zero−zero frequency. The experimental dimer spectra exhibit the reduced Franck−Condon activity expected from distributing the electronic excitation over two monomers. However, deviations in the intensity patterns for individual vibrations suggest additional, more specific effects of dimerization, and the electronic transition moment for the lowest allowed transition of the monomer is not conserved upon dimer formation. An excitonically coupled monomer model therefore appears inadequate to describe the electronic excitations in these strongly coupled noncovalent dimers.

1. Introduction

The optical properties of noncovalent molecular aggregates are important in a variety of natural and technological contexts including photosynthesis, photography, molecular electronics, and nonlinear optical materials. These aggregates may have well-defined geometries on the nanoscale but lack long-range crystalline order. The interchromophore interactions are sufficiently strong that the optical properties of the aggregate are considerably different from those of the isolated monomers, yet weak enough that individual molecules can be considered to retain their identity. The simplest models for the electronic spectroscopy of such aggregates ignore the possibility of electron transfer or exchange between monomers and treat the intermolecular interaction as a multipole expansion of the charge distributions on each monomer. For strongly allowed electronic transitions, the dominant term is the coupling between transition dipole moments on the constituent monomers, which splits the *N* initially degenerate electronic excitations on *N* monomers into a band of transitions whose energies and oscillator strengths depend on the positions and relative orientations of the interacting monomers.[1−12]

For small aggregates of specified geometry it is straightforward to calculate the spectra within these approximations as long as the absorption spectrum of each monomer is treated as a single transition. Real molecular spectra have vibronic structure, and inclusion of vibronic effects, even within a simple harmonic model, considerably complicates the analysis. Long ago, Fulton and Gouterman carried out calculations of absorption spectra of a simple molecular homodimer with inclusion of one linearly coupled harmonic vibration.[1] They showed that, when the intermolecular coupling is very weak (e.g., the distance between monomers is large), the absorption spectrum resembles that of the monomer but with each vibronic transition split into two lines. When the coupling is strong, there are two widely separated electronic transitions each possessing what appears to be a normal vibronic progression, but with reduced Franck−Condon activity consistent with the electronic excitation being spread over both monomers. For intermediate coupling the vibronic structure is strongly perturbed and does not follow any simple Franck−Condon progression. We recently developed this model for the more general situation in which each monomer has multiple vibrational modes coupled to the electronic transition. We also examined resonance Raman excitation profiles and depolarization ratios as well as hyper-Rayleigh scattering intensities for this model.[11]

The present work represents an effort to test these theoretical predictions for dimers. It is difficult to find molecules that can be studied readily in both monomeric and dimeric forms at known concentrations with minimal spectral interference from the other form. The Bazan group, for example, has synthesized a number of covalent dimers based on stilbene and distyrylbenzene chromophores linked through a paracyclophane moiety,[13−18] but in these systems the intermonomer interactions are sufficiently strong that the "dimer" has to be treated as a completely new molecule rather than as excitonically coupled monomers. Covalent linear porphyrin arrays are promising candidates for the study of excitonic interactions, but their spectroscopy is complicated by the reduced local symmetry of the arrays compared with the highly symmetric monomers.[19−23] Noncovalent dimers should have weaker interactions and are closer to the actual systems of interest, but whereas many molecules are monomeric at low concentrations and aggregate

† Part of the special issue "Gerald Small Festschrift".
‡ University of California.
§ Universität Würzburg.

10.1021/jp037371x CCC: $27.50
Published on Web 02/12/2004

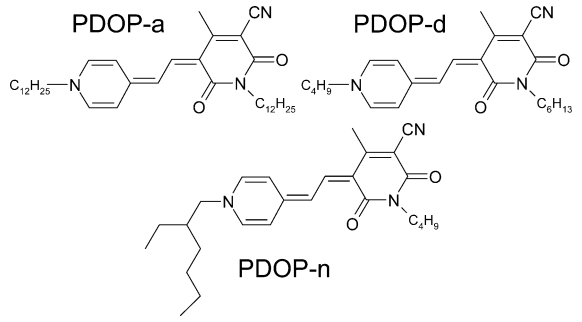

Figure 1. Structures of merocyanine dyes.

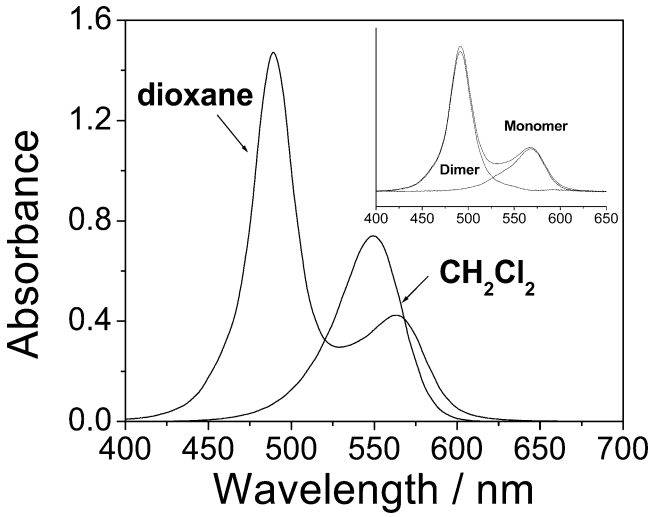

Figure 2. Absorption spectra of PDOP-d in CH_2Cl_2 (monomeric) and in dioxane (primarily dimeric). The inset shows the decomposition of the dioxane spectrum into pure monomer and pure dimer spectra. The monomer absorption is blue-shifted in CH_2Cl_2 compared with dioxane.

at higher concentrations, the solutions usually contain a complicated mixture of monomers, dimers, and larger aggregates. A number of oxazine dyes aggregate in predominantly dimeric form on SiO_2 and SnO_2 surfaces, but straightforward comparison with the monomer in solution is complicated by the additional effects of binding to the surface.[24−26] Recently, Würthner and co-workers reported the synthesis and characterization of a set of merocyanine dyes that exhibit very clean monomer−dimer equilibria with little interference from higher aggregates in appropriate solvents.[27] The equilibrium constants for dimer formation and the electronic spectra of the monomers and dimers were obtained, along with information on the structure of the dimers. The electronic spectra of the dimers were interpreted using a simple excitonic-coupling model without inclusion of vibronic effects.

In this work, we examine both the electronic absorption spectra and the resonance Raman excitation profiles and absolute cross sections for three of these pyridine−dimethine−oxypyridone (PDOP) dyes (Figure 1). PDOP-a and PDOP-d are structures **1a** and **1d**, respectively, of ref 27. PDOP-n was not studied in that work but has similar properties. All three molecules share a common conjugated skeleton and have nearly identical electronic absorption spectra. The differing alkyl substituents on the nitrogens do, however, influence the dimerization equilibria. The concentration-dependent absorption spectra in dioxane are fully consistent with a monomer−dimer equilibrium, $2M \leftrightarrows M_2$, with the dimer absorption spectrum blue-shifted relative to that of the monomer by roughly 2700 cm^{-1} (see Figure 2). AM1 geometry optimizations and 2D NMR ROESY (rotating-frame Overhauser enhancement spectroscopy) experiments were performed on the dimer of the analogue of PDOP-n in which another ethylhexyl group replaces the *n*-butyl group, and the results were consistent with a face-to-face antiparallel dimer structure. Electrooptic absorption measurements on another analogue having different alkyl substituents yield ground- and excited-state dipole moments of 17.1 and 12.6 D, respectively, for the monomer in dioxane. All of the available data suggest that these molecules should be excellent examples of noncovalent, excitonically coupled H-dimers in solution.

2. Experimental Methods

The syntheses of PDOP-a and PDOP-d were described in ref 27. PDOP-n was synthesized by the method reported in ref 27 and isolated by chromatography on silica gel with dichloromethane/methanol (94:6) and recrystallization from acetic acid to give violet crystals (yield 90%). Mp 187−188 °C; ^{1}H NMR (500 MHz, $CDCl_3$) δ = 7.75 (d, J = 14.9 Hz; 1H), 7.57 (d, J = 7.4, 2H), 7.54 (d, J = 14.9 Hz, 1H), 7.21 (d, J = 7.1 Hz, 2H), 4.06 (m, 2H), 3.97 (t, J = 7.7 Hz, 2H), 2.31 (s, 3H), 1.80 (m, 1H), 1.62 (m, 2H), 1.29−1.43 (m, 10H), 0.95 (m, 6H), 0.90 ppm (t, J = 6.7, 3H). Anal. Calcd for $C_{26}H_{35}N_3O_2$ (421.6): C, 74.07; H, 8.37; N, 9.97. Found: C, 73.92; H, 8.31; N, 9.76. Spectroscopic grade dioxane (Fisher) and dichloromethane (Fisher) were used as received.

Concentration-dependent absorption spectra were measured and fit to a monomer−dimer equilibrium[27] to obtain the spectra of the monomeric and dimeric forms of the chromophores in dioxane. The resonance Raman spectra of the dimers were obtained in dioxane at concentrations of 30−80 μM.[28] At these concentrations the monomer still makes an observable contribution to the absorption spectrum, but as the Raman excitation wavelengths are much more strongly resonant with the dimer absorption, the dimer dominates the spectra. Calculations described in section 5 below support this assumption. We were not, however, able to obtain adequate resonance Raman spectra of the monomers in dioxane. Even at concentrations as low as 1 μM the absorption spectra show a nonnegligible dimer contribution, and the strong monomer fluorescence requires that the Raman spectra be excited on the blue edge of the absorption where any dimer contribution is strongly enhanced. We therefore obtained the monomer spectra in CH_2Cl_2, a considerably more polar solvent in which negligible dimer formation is observed at concentrations below 1 mM. The resonance Raman spectra of the monomers were obtained at concentrations of 0.5−0.7 mM.

Absorption spectra were measured on a Hitachi U-3010 UV−vis spectrophotometer. Infrared absorption spectra were obtained on a Nicolet Protégé 460 FTIR spectrometer from samples evaporated from dioxane or CH_2Cl_2 solution onto polyethylene ST-IR cards (Thermo Electron). Raman spectra were obtained on a Spex 1877 triple spectrograph equipped with a Spex Spectrum One liquid nitrogen cooled CCD (charge-coupled device). Raman spectra were excited with 10−20 mW of average power from either a Lexel CW argon-ion laser or a frequency-doubled Spectra-Physics Tsunami Ti:sapphire laser producing ~10 ps pulses at 82 MHz. Samples of about 2 mL volume were contained in a rotating cylindrical cell, and the Raman scattering was collected in a ~135° backscattering geometry. The scattered light was passed through a polarization scrambler and collected and focused onto the spectrograph entrance slit with an ellipsoidal mirror. Spectra were corrected for reabsorption and for the wavelength dependence of the spectrograph throughput and detector sensitivity.[29] Integrated peak areas were determined by fitting regions of the spectrum to sums of mixed Gaussian−Lorentzian peaks (Grams32) after

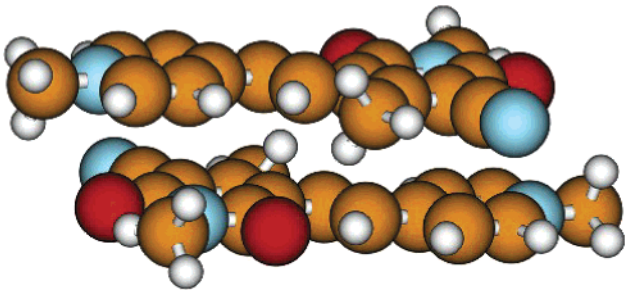

Figure 3. Geometry of the H-dimer obtained from an energy minimization with the AM1 method. The alkyl groups on the structures of Figure 1 have been replaced by methyl groups.

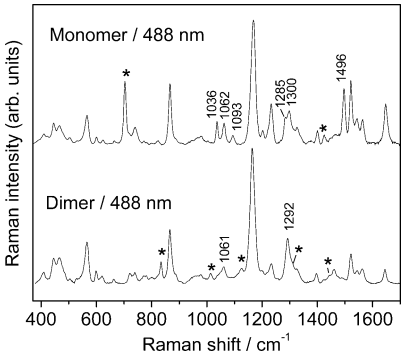

Figure 4. Resonance Raman spectra of PDOP-d in monomeric form in CH_2Cl_2 (top) and in predominantly dimeric form in dioxane (bottom). The excitation wavelength for both spectra is 488.0 nm. Asterisks mark solvent lines.

subtraction of a low-order polynomial to remove underlying fluorescence.[30] The *x*-axes were calibrated using dioxane solvent Raman lines as a standard. Spectral resolution was 5−7 cm^{-1}. The absolute differential resonance Raman cross sections ($d\sigma/d\Omega$) were determined by measuring the integrated areas of the chromophore Raman bands relative to that of the 702 cm^{-1} line of the CH_2Cl_2 solvent (for the monomer) or the 835 cm^{-1} line of the dioxane solvent (for the dimer) as internal standards.[31] The absorption and Raman cross sections for the dimer are reported on a *per dimer* basis in all cases.

3. Computational Methods

The absorption and resonance Raman spectra of the monomers were simulated via the time domain wave packet method.[29,31,32] The ground and electronically excited potential energy surfaces were treated as a collection of simple displaced harmonic oscillators having equal frequencies in both states. No mixing of the normal modes (Duschinsky rotation) or coordinate dependence of the electronic transition moment was considered. The broadening of the electronic absorption spectra was divided into inhomogeneous broadening, modeled as a static Gaussian distribution of electronic zero−zero energies, and homogeneous broadening, modeled either as an exponential decay in the time domain or as the decay function obtained by assuming coupling of the electronic transition to an overdamped Brownian oscillator. The parameters describing the monomer's electronic transition were adjusted to obtain the best simultaneous fit to the absorption spectrum and the absolute resonance Raman cross sections. The calculations included 24 to 30 vibrational modes between 400 and 1700 cm^{-1} observed in the resonance Raman spectra. Lines that were too strongly overlapped to be separated reliably were combined into a single frequency for modeling purposes.

Two different approaches were used to model the dimer spectra. First, the dimer was treated as a supermolecule in the same manner as the monomer. This approach should be appropriate in the limit of strong electronic coupling, where simple harmonic vibrational progressions are recovered. The other approach was to model the dimer as two monomers coupled through the dipole−dipole interaction of their electronic transition moments.[11] We assumed that the two monomers are stacked coplanar with their transition dipoles exactly antiparallel (Figure 3), resulting in nonzero oscillator strength in only the higher-energy of the two electronic transitions (a "pure" H-dimer). Some of the other PDOP dyes studied in ref 27 also exhibit a weak low-energy J-band in some solvents, but this band is very weak or absent in the three molecules studied here. The slip angle (the angle between the dipole direction and a line connecting the two centers, θ in ref 11 and α in ref 27) was estimated as 60°. The distance between the molecular centers was left as an adjustable parameter. Because of the need to perform these calculations in the frequency domain, the electronic dephasing function was assumed to be pure exponential decay although this is unrealistic for molecules in fluid solution. Also, for the Raman calculations the modes other than the Raman-active one were lumped into four effective modes such that the total reorganization energy for each frequency group was held constant. The details of the computational methods are described elsewhere.[11,26]

Density-functional theory (DFT) calculations of the ground-state geometry and vibrational frequencies of the monomer were carried out using the B3LYP hybrid density functional and the 6-311G** basis set as implemented in Gaussian 98.[33] Ground-state geometries were calculated for both monomers and dimers with the AM1 semiempirical Hamiltonian. In addition, the ZINDO method was used to calculate the electronic transition energies and oscillator strengths of dimers in which the intermolecular distance was varied. These calculations employed configuration interaction among all singly excited configurations involving the 29 highest occupied and 29 lowest virtual orbitals. All calculations were performed on a truncated chromophore in which the alkyl groups on the ring nitrogens were replaced by methyls (see Figure 3). The three chromophores in Figure 1, which differ only in the identities of these alkyl groups, have very similar resonance Raman spectra. The density-functional and semiempirical methods both give essentially planar geometries for the monomer, but the DFT geometry has nearly equal bond lengths for the three CC bonds in the polyenic linker, whereas the AM1 geometry has more bond order alternation (the central "single" bond in the structures shown in Figure 1 is about 0.04 Å longer than the two neighboring "double" bonds).

4. Results

Figure 4 shows representative resonance Raman spectra of PDOP-d in its monomeric and dimeric forms. Most of the Raman lines have comparable relative intensities and frequencies that differ by no more than 2−3 cm^{-1}. However, the monomer lines at 1496, 1093, and 1036 cm^{-1} apparently disappear altogether in the dimer. Some intensity changes are expected because of the large blue-shift in the absorption spectrum upon dimerization. The excitation wavelength of 488 nm is near the absorption maximum of the dimer but far to the blue side of the monomer spectrum, and because the excitation profiles for higher-frequency vibrations are generally blue-shifted relative to those for lower-frequency modes, the increased relative intensity in the 1450−1650 cm^{-1} region in the monomer is expected. However, these general patterns of excitation wavelength dependence do not explain the complete disappearance

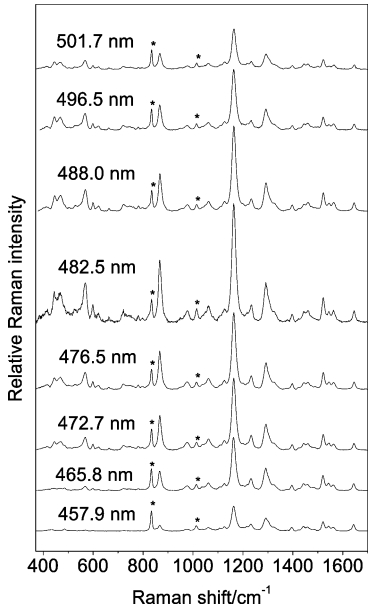

Figure 5. Resonance Raman spectra of PDOP-a in dioxane (predominantly dimers, the dimer concentration is 36.5 μM) at the indicated excitation wavelengths. Fluorescence backgrounds have been subtracted. All spectra are scaled to have approximately equal intensities in the 835 cm^{-1} solvent line, and the *y*-axes are offset arbitrarily. The asterisks mark lines due primarily to dioxane solvent.

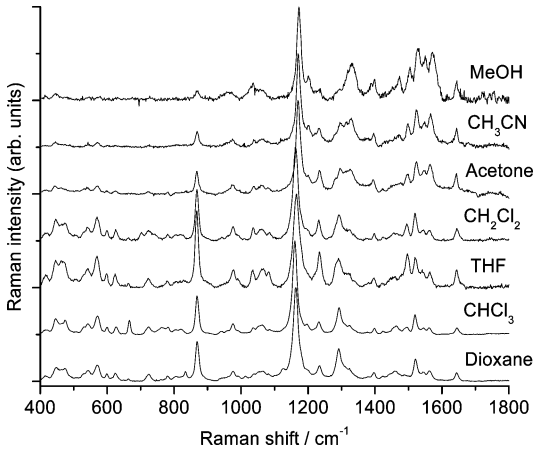

Figure 6. Resonance Raman spectra of PDOP-n in different solvents. The excitation wavelengths are 457.9 nm for methanol, 476.5 nm for CH_3CN and acetone, and 488.0 nm for the other four solvents. Relative intensities and *y*-axis offsets are arbitrary. The absorption maxima of the monomers are 566 nm in dioxane, 561 nm in $CHCl_3$, 552 nm in THF, 550 nm in CH_2Cl_2, 527 nm in acetone, 516 nm in CH_3CN, and 495 nm in methanol. The absorption spectra indicate that the samples are primarily dimers in dioxane, a mixture of monomers and dimers in $CHCl_3$, and almost entirely monomers in the other five solvents.

of some strong monomer lines in the dimer, implying that dimerization must produce some more specific vibrational effects.

Figure 5 gives an overview of the resonance Raman spectra of PDOP-a in its dimeric form as a function of excitation wavelength. This figure shows that the Raman intensities of most of the modes reach their maxima at excitation wavelengths slightly to the blue of the dimer absorption maximum (near 490 nm).

Figure 6 shows the resonance Raman spectrum of PDOP-n in seven different solvents spanning a wide range of polarities. The absorption maxima of the monomer in each solvent are given in the figure legend and range from 566 nm in dioxane to 495 nm in methanol. This blue-shift with increasing solvent polarity is consistent with a reduction in the permanent dipole moment upon electronic excitation as discussed previously.[27]

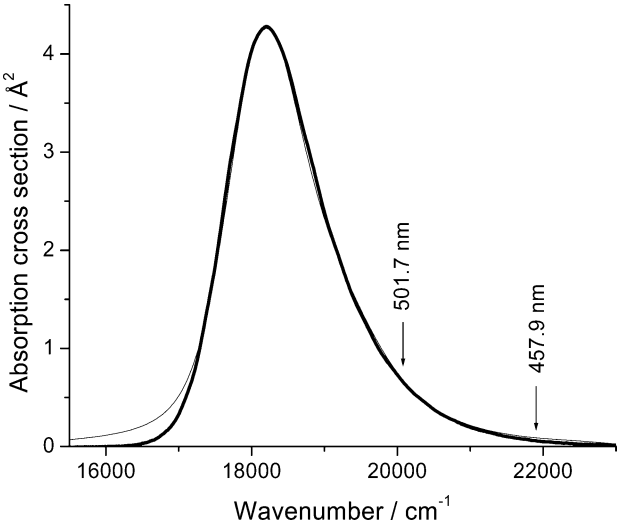

Figure 7. Absorption spectrum of PDOP-d monomer in CH_2Cl_2 (thick line) and the spectrum calculated from the model parameters of Table 1 (thin line). The Raman excitation wavelength range is indicated.

TABLE 1: Experimental and Calculated Resonance Raman Cross Sections for the Monomer of PDOP-d in CH_2Cl_2 (Exponential Dephasing Model)[a]

	Raman cross section/10^{-11} Å^2 sr^{-1} at					
	501.7 nm		496.5 nm		488.0 nm	
freq/cm^{-1}	exptl	calcd	exptl	calcd	exptl	calcd
410	81	93	69	74	61	45
445	218	222	187	178	101	109
466	197	202	165	163	122	101
503	37	43	21	34	18	21
566	212	222	186	179	116	115
600	33	31	18	25	15	16
624	27	26	18	21	12	13
866	421	455	320	338	247	227
980	277	281	185	196	118	129
1036	163	172	107	116	74	75
1062	260	278	168	186	117	117
1093	73	82	56	54	33	33
1168	1551	1639	1042	1055	744	621
1202	82	93	59	59	44	34
1233	446	454	287	288	187	162
1285	248	258	160	162	106	88
1300	398	401	257	252	141	135
1325	239	240	154	151	76	80
1400	117	125	69	79	47	40
1496	366	392	267	256	154	134
1520	452	482	321	318	183	153
1545	161	178	116	118	66	57
1564	184	202	134	136	83	65
1647	281	295	210	209	97	101

[a] Parameters for the calculations are given in Table 2.

The solvent-dependent spectra were not modeled quantitatively but were used only to aid in interpreting the changes in the vibrational spectrum upon dimerization. Specifically, these data suggest that the intensity changes observed upon dimerization are not simply effects of changing the local polarity; the 1036 and 1496 cm^{-1} modes are clearly observable in all of the solvents in which the monomer is the dominant form (methanol, acetonitrile, acetone, methylene chloride, and THF) but are much weaker in a mixture of monomers and dimers (chloroform) and are absent when the dimer predominates (dioxane).

The absorption spectrum and the resonance Raman cross sections at five wavelengths from 458 to 501 nm were simultaneously modeled to extract the excited-state parameters for the monomers in CH_2Cl_2. Figure 7 and Table 1 compare the experimental and calculated absorption spectrum and resonance Raman intensities for PDOP-d, calculated assuming

TABLE 2: Model Parameters for the Monomers and Dimers of the Three Chromophores (Single Electronic Transition, Exponential Dephasing Model)

PDOP-a				PDOP-d				PDOP-n			
monomer		dimer		monomer		dimer		monomer		dimer	
freq	Δ	freq	Δ	freq	Δ	freq	Δ	freq	Δ	freq	Δ
										395	0.03
413	0.246	413	0.055	410	0.31	409	0.085	421	0.34	416	0.06
443	0.256	446	0.089	445	0.44	445	0.07	445	0.226	447	0.098
463	0.331	470	0.095	466	0.4	467	0.137	463	0.492	463	0.112
										474	0.067
499	0.127	504	0.038	503	0.17	504	0.034	507	0.098	509	0.047
		529	0.056			527	0.024			528	0.029
								542	0.22	543	0.118
568	0.312	568	0.109	566	0.34	567	0.144	570	0.275	571	0.105
598	0.089	598	0.051	600	0.12	599	0.048	600	0.126	600	0.064
621	0.12	621	0.041	624	0.105	618	0.051	627	0.123	625	0.073
										650	0.01
661	0.05	664	0.024			665	0.037			664	0.022
		722	0.085			722	0.05			724	0.065
						739	0.069				
						770	0.051			762	0.017
782	0.097	782	0.031			781	0.041			781	0.044
		797	0.048			798	0.037			805	0.039
824	0.073	823	0.04			823	0.067			823	0.057
867	0.295	867	0.144	866	0.29	866	0.151	869	0.298	869	0.146
978	0.166	978	0.067	980	0.188	978	0.109	977	0.194	977	0.078
1035	0.143			1036	0.134			1036	0.138		
1060	0.191	1063	0.09	1062	0.163	1061	0.105	1062	0.143	1065	0.099
1102	0.081			1093	0.084			1086	0.122		
1166	0.359	1163	0.27	1168	0.333	1165	0.296	1167	0.358	1164	0.27
1200	0.082			1202	0.075						
1231	0.178	1234	0.088	1233	0.158	1233	0.096	1233	0.17	1235	0.091
1284	0.066			1285	0.11			1283	0.12		
1296	0.19	1292	0.146	1300	0.134	1292	0.162	1299	0.135	1292	0.156
1326	0.102	1325	0.084	1325	0.1	1321	0.103	1325	0.095		
1398	0.075	1398	0.057	1400	0.065	1396	0.06	1400	0.064	1398	0.044
		1424	0.032			1422	0.044				
		1461	0.079			1487	0.066			1460	0.088
1495	0.137			1496	0.102			1496	0.105		
1519	0.131	1522	0.101	1520	0.11	1521	0.12	1520	0.13	1522	0.101
1542	0.099	1545	0.08	1545	0.065	1543	0.087	1545	0.076	1544	0.072
1560	0.09	1563	0.072	1564	0.068	1563	0.095	1564	0.075	1565	0.075
1645	0.09	1645	0.073	1647	0.076	1643	0.087	1647	0.095	1645	0.07
$\lambda_{vib} = 366$ cm^{-1}		$\lambda_{vib} = 125$ cm^{-1}		$\lambda_{vib} = 370$ cm^{-1}		$\lambda_{vib} = 161$ cm^{-1}		$\lambda_{vib} = 384$ cm^{-1}		$\lambda_{vib} = 130$ cm^{-1}	
$\mu_{ge} = 2.56$ Å		$\mu_{ge} = 3.22$ Å		$\mu_{ge} = 2.58$ Å		$\mu_{ge} = 3.38$ Å		$\mu_{ge} = 2.62$ Å		$\mu_{ge} = 3.25$ Å	
$\Gamma = 250$ cm^{-1}		$\Gamma = 210$ cm^{-1}		$\Gamma = 250$ cm^{-1}		$\Gamma = 240$ cm^{-1}		$\Gamma = 250$ cm^{-1}		$\Gamma = 270$ cm^{-1}	
$\sigma_{inh} = 360$ cm^{-1}		$\sigma_{inh} = 380$ cm^{-1}		$\sigma_{inh} = 350$ cm^{-1}		$\sigma_{inh} = 380$ cm^{-1}		$\sigma_{inh} = 350$ cm^{-1}		$\sigma_{inh} = 350$ cm^{-1}	
$E_0 = 18\,120$ cm^{-1}		$E_0 = 20\,330$ cm^{-1}		$E_0 = 18\,080$ cm^{-1}		$E_0 = 20\,430$ cm^{-1}		$E_0 = 18\,040$ cm^{-1}		$E_0 = 20\,330$ cm^{-1}	

Lorentzian homogeneous line widths (exponential decay). The simulation parameters are given in Table 2. The absorption spectra are fit quite well except for an excessively broad Lorentzian wing on the red edge of the calculated spectrum. Calculations utilizing the overdamped Brownian oscillator dephasing function[29,34] give much better fits to the low-energy edge with only small changes in the vibrational displacement parameters. Because of interference from the weakly Stokes-shifted fluorescence of the monomers, resonance Raman data could be obtained only with excitation far to the blue of the absorption maximum. The intensities in this region are reproduced quite well. The change in geometry upon excitation is small, and the solvent-broadened electronic origin is by far the strongest single feature in the absorption spectrum. The vibrational reorganization energy, $\lambda_{vib} = \sum_i(\omega_i\Delta_i^2/2)$, is only 366 cm^{-1}, and most of the vibrations with significant Franck−Condon activity are at fairly low frequencies which are hard to distinguish from the broadened origin. Results similar to those of Figure 7 and Table 1 were obtained for the other two chromophores, whose simulation parameters are also given in Table 2.

The absorption spectrum of monomeric PDOP-d in dioxane is somewhat narrower than that in CH_2Cl_2 and is red-shifted by about 550 cm^{-1}. A good fit to the monomer absorption spectrum in dioxane (except on the red edge as discussed above) is obtained by using the CH_2Cl_2 fitting parameters of Table 2 with the inhomogeneous line width reduced from 350 to 273 cm^{-1}, the homogeneous line width increased from 250 to 300 cm^{-1}, the zero−zero energy shifted to 17 520 cm^{-1}, and the electronic transition length increased from 2.58 to 2.75 Å.

One approach to modeling the dimer is to treat it as a supermolecule in the same manner as the monomer, a single allowed electronic transition linearly coupled to harmonic vibrations. Figure 8 compares the experimental and calculated absorption spectra for the dimer of PDOP-n, and Figure 9 compares the experimental resonance Raman cross sections with the calculated excitation profiles for six of the strongest vibrations. The fits to both the absorption spectrum and the Raman profiles are reasonably good. Similar results were obtained for the other two chromophores. Table 2 compares the best-fit parameters for each of the three chromophores. The dimers show several weak lines between 650 and 850 cm^{-1}, a frequency range which is obscured by the strong C−Cl stretches of the solvent in the monomer. These lines may be present in the monomers as well, but they are so weak that their omission

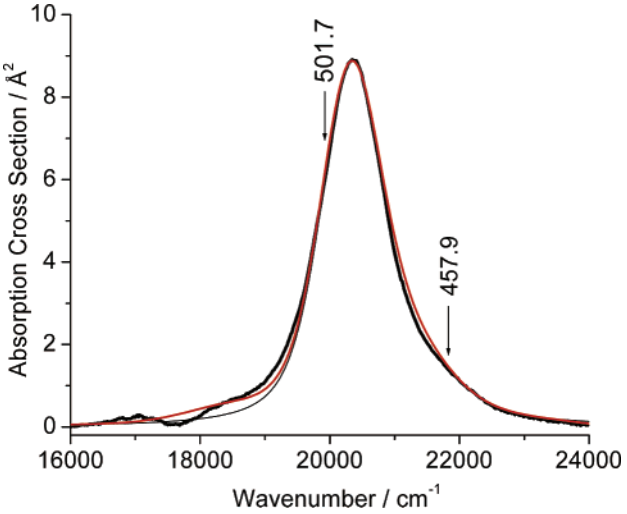

Figure 8. Absorption spectrum of PDOP-n dimer in dioxane (thick black curve), the spectrum calculated from the dimer-as-supermolecule parameters of Table 2 (thin black curve), and the spectrum calculated from the explicitly coupled monomers model (red curve). The Raman excitation wavelength range is indicated.

from the monomer fits has an insignificant effect on the modeling of the absorption spectrum and the Raman profiles for the other modes.

The dimer spectra were also modeled explicitly as excitonically coupled monomers.[11,26] We started with the vibrational frequencies and displacements from the monomer fitting parameters of Table 2. The vibrations were divided into four frequency groups and each group was represented by one effective mode having an average frequency and a reorganization energy equal to the total for that group. These four modes were used to simulate the dimer absorption spectrum with the zero−zero energy fixed to the monomer value (adjusted to account for the pure solvent shift between methylene chloride and dioxane) and the other parameters set equal to the Table 2 monomer values. The ground- and excited-state permanent dipole moments were taken to be 17.1 and 12.6 D, respectively,[27] and the intermonomer separation was varied to obtain the best fit to the dimer absorption spectrum (adjusting the intermonomer coupling to reproduce the experimental blue-shift). The dimer absorption spectrum is fit very well with this method. Each Raman profile was then calculated from this set of parameters by adding the mode of interest, with its own Δ as determined for the monomer, and reducing the Δ in the mode representing the group to which that mode belongs so as to hold the total reorganization energy constant. This procedure resulted in rather poor calculated Raman intensities, in error by factors of 2−3 in many of the modes as shown in Figure 9. We therefore tried a second approach that started from the vibrational parameters of Table 2 for the *dimer* treated as a supermolecule. Each vibrational displacement was then increased by $\sqrt{2}$ to account for the expected change in electron−phonon coupling between the monomer and the strongly coupled dimer. The spectra were then simulated as described above with the line widths set equal to the Table 2 dimer values and the transition dipole set to the Table 2 dimer value divided by $\sqrt{2}$. Table 3 summarizes the parameters used for all three molecules. Both the absorption spectra and, particularly, the Raman profiles generated from this calculation are nearly indistinguishable from those produced by the full 30-mode dimer parameters of Table 2. This shows that we are in the "strong intermolecular-coupling" regime where the splitting between the two members of the excitonically coupled transition (only one of which has

TABLE 3: Simulation Parameters for Dimers Treated as Excitonically Coupled Monomers[a]

molecule	PDOP-a	PDOP-d	PDOP-n
E_0/cm^{-1}	17 640	17 580	17 640
μ_{ge}/Å	2.32	2.44	2.34
μ_g/Å	3.56	3.56	3.56
μ_e/Å	2.63	2.63	2.63
Γ/cm^{-1}	210	240	270
σ_{inh}/cm^{-1}	380	380	350
R_{ab}/Å	4.66	4.69	4.68

[a] Vibrational frequencies are the same as the dimer column in Table 2, and Δ values are those of Table 2 multiplied by $\sqrt{2}$.

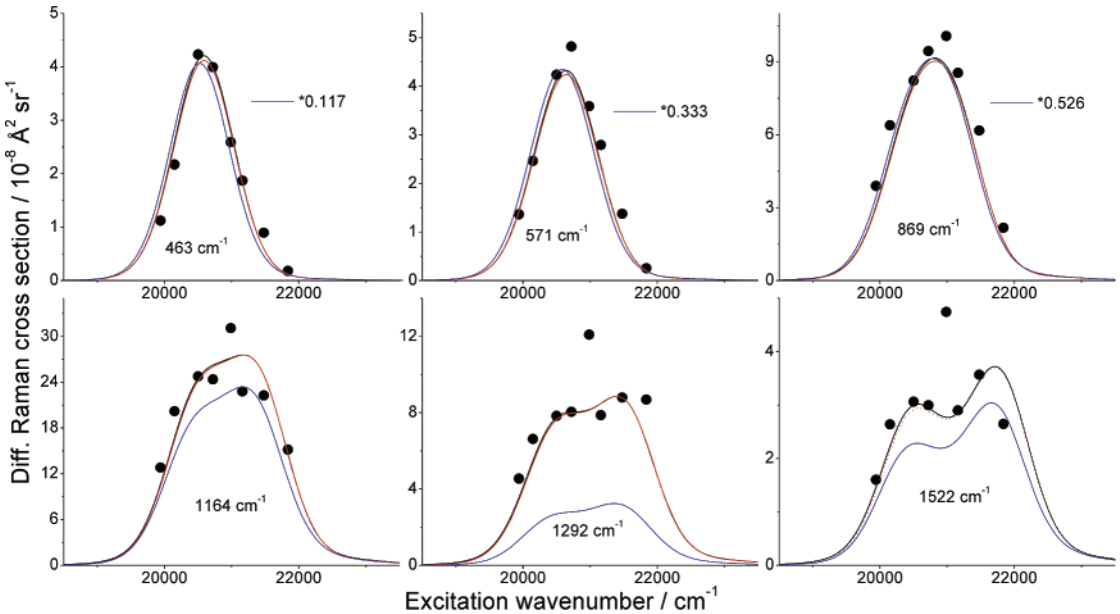

Figure 9. Experimental resonance Raman cross sections for the indicated vibrations of the PDOP-n dimer in dioxane (points), excitation profiles calculated from the dimer-as-supermolecule model parameters of Table 2 (black curve), and profiles calculated as excitonically coupled monomers with the monomer vibrational parameters (blue curve), and the rescaled dimer vibrational parameters (red curve) as described in the text. Note the scaling factors applied to the blue curve in three of the profiles. The estimated uncertainties in the experimental cross sections are ±20%.

TABLE 4: Experimental (Raman and IR) and Calculated (B3LYP/6-311G) Vibrational Frequencies for PDOP-n[a]**

exptl freq/cm^{-1}					
Raman in		FTIR evap from		calcd freq/cm^{-1}	
CH_2Cl_2 (monomer)	dioxane (dimer)	CH_2Cl_2	dioxane	(IR intensity)	calcd normal mode description
	395			382	N-alkyl and C−C═O bend
421	416			406 vw	A ring C−C═O bend and C−Me bend
445	447	440 vw	437 vw	437 w	A ring def
463	463			451 vw	A ring def
	474			471	C_e−D ring bend
507	509	515 vw	516 vw	501	A ring C−C≡N bend
	528			542	A ring oop def
542	543	544 vw		512	D ring def
570	571			595	A ring oop def
600	600			622 vw	A ring sym breathe/def
627	625	625 vw	626 vw	658 vw	A ring def
	650			674	D ring asym def
	664			703	H oop w
	724			748 vw	A ring def, C−C≡N bend, C−C═O bend
	762			774	H oop w
	781	781 w	780 w	789 w	D ring sym breathe, N-alkyl str
	805			806	H oop w
	823			823 w	H oop w
869	869	871 w, b	871 w	864 w	D ring sym breathe
		953 m, b	957 w	905−975 vw	H oop w
977	977			985 w	A ring def, C−Me str, N−C str
1036		1036 m	1036 m	1036	D ring trigonal def
1062	1065	1059 m	1052 m	1065/1072 w	Alkyl H r
1086				1087 vw	Alkyl H r
1167	1164	1170 vs	1171 vs	1216 s	D ring sym CH r, D ring N−Me str
		1221 m	1220 m	1231 m	A ring asym C−C, C_e-H r
1233	1235			1246 w	D ring N-Me str
1283				1286 m	C_e−C_e str, C_e−H r
1299	1292	1296 s	1295 s	1335 s	A ring N-alkyl, C−Me and CC str
		1312 w	1314 w	1346 w	C_e−H r, D ring CH r, C−C str
1325		1328 m	1328 m	1361 s	C_e−H r, A ring C−C, N−C str
		1377 w	1374 w	1386 vw	D ring asym N−C
1400	1398	1397 w	1394 w	1411−1470 s	Alkyl H defs
	1460			1487−1519 w	Alkyl H defs
1496		1493 vs	1490 vs	1547 m	C_e−D ring str, D ring N−C sym str, D ring N-alkyl str
1520	1522	1523 m	1522 m	1560 vs	C_e−A ring str, C_e−C_e str, D ring antiquinoidal str
1545	1544	1541 vw	1542 vw	1573 vs	D ring antiquinoidal str, C_e−A ring str
1564	1565	1566 m	1560 m	1614 m	A ring C(Me)−C(CN) str, C_e−C_e str
		1592 s	1587 s	1694 s	Asym C═O str
1647	1645	1645 m	1646 m	1701 m	D ring quinoidal str

[a] Abbreviations: D, donor (alkylpyridine ring); A, acceptor (ring containing C═O groups); C_e, central "ethylenic" carbon; (a)sym, (anti)symmetric; str, stretch; def, deformation; r, rock; oop, out-of-plane; w, wag. All normal modes are in-plane unless otherwise noted. IR intensities are given qualitatively as very strong (vs), strong (s), medium (m), weak (w), or very weak (vw).

oscillator strength in a pure H-dimer) is so large that each transition exhibits a normal harmonic vibrational progression.[1]

The dioxane solutions from which the "dimer" Raman data were obtained do contain some free monomer. We have obtained the dimer concentration in each solution by fitting the absorption spectrum to a weighted sum of the pure monomer and pure dimer spectra. All of the Raman intensity in the dioxane solutions is assumed to come from the dimer. This is a reasonable assumption because the excitation wavelengths employed are much more strongly resonant with the dimer than with the monomer (compare Figures 7 and 8). To test this, we calculated the Raman intensities expected from the monomer in dioxane by using the monomer modeling parameters of Table 2, shifting the zero−zero energy to account for the red-shift between CH_2Cl_2 and dioxane. In the worst case, the highest frequency vibrations at the reddest excitation wavelengths, the residual monomer should account for no more than 6% of the total measured intensity.

Infrared absorption spectra were obtained for PDOP-n as thin films evaporated from both dioxane and CH_2Cl_2. Table 4 summarizes the IR frequencies and qualitative intensities and compares them with the Raman frequencies. Also shown are tentative assignments, made by comparing both frequencies and IR intensities, to the vibrational frequencies and normal mode descriptions calculated from density-functional theory. The exact physical state of the chromophores in these films produced by rapid solvent evaporation is not known, and clearly neither sample corresponds to isolated monomers. The samples prepared from the different solvents show similar overall intensity patterns and small frequency shifts. Significantly, the two lines that are strong in the Raman spectra of the monomers but absent from the dimer spectra (1496 and 1036 cm^{-1}) are fairly intense in both IR spectra.

Finally, semiempirical calculations were performed in order to evaluate the assumption that an excitonically coupled monomer model is adequate, that is, that the electrons remain associated with a single monomer and orbital overlap between monomers can be neglected. If orbital overlap becomes significant, the dimer must be considered a new molecule with properties distinct from those of the monomers. We carried out ZINDO calculations of the electronic transition energies and oscillator strengths of dimers that were constructed by starting from the AM1-minimized dimer geometry (molecular planes separated by 3.5 Å) and moving the monomers farther apart

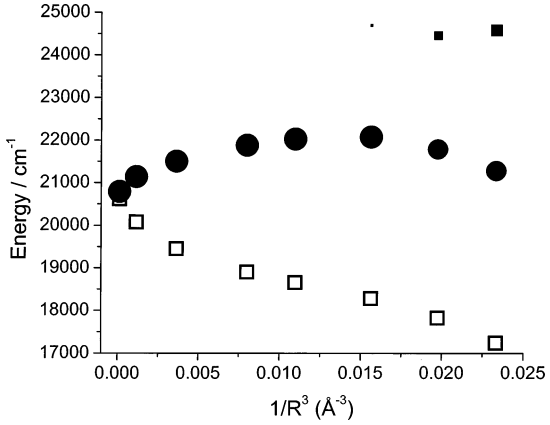

Figure 10. ZINDO/CI-calculated energies of the two lowest electronic states of the dimer (open squares and filled circles) and the next lowest state having oscillator strength $f > 0.1$ (filled squares), as a function of the inverse cube of separation between the intermolecular planes. The areas of the filled symbols are proportional to their oscillator strengths.

without changing the monomer geometries. Figure 10 summarizes the most important results. At large intermonomer separations two nearly degenerate electronic transitions are calculated near 480 nm: a forbidden one corresponding to the J-transition and a strongly allowed one corresponding to the H-transition. The next transition with significant oscillator strength is more than 20 000 cm^{-1} higher in energy. As the monomers are brought closer together, the splitting between the forbidden and allowed transitions increases rapidly while the oscillator strength and the MO/CI descriptions of these states remain nearly unchanged. At distances of 4 Å or less, however, the splitting between the two lowest transitions ceases to increase, the oscillator strength of the H-band begins to decrease (from $f = 3.4$ at $R \geq 4.5$ to $f = 2.2$ at 3.5 Å), and the intensity lost from the H-band appears in a new transition shifted about 3000 cm^{-1} to the blue. These results suggest that an excitonically coupled monomer picture is reasonable for interplane separations greater than about 4.5 Å but breaks down at shorter distances.

5. Discussion

The raw spectroscopic data, as well as the results of the spectral simulations, are qualitatively consistent with the expectations of the excitonically coupled monomer model. The absorption spectrum of the dimer is strongly blue-shifted and somewhat narrowed compared with that of the monomer, as expected for H-type dimers. The modeling parameters of Table 2 show that the narrowing of the spectrum results mainly from the reduced coupling of vibrations to the electronic transition. Most of the displacements (Δ) are reduced in the dimers, while the homogeneous and inhomogeneous line widths are fairly constant. This result is also consistent with simple exciton-coupling theory, which predicts that all of the monomer's vibrational displacements should be reduced by a factor of $\sqrt{2}$ upon dimerization in the strong excitonic-coupling limit. The vibrational reorganization energy for the monomer should therefore be twice that of the dimer. We obtain somewhat greater differences in λ_{vib} of 2.3−2.9 between monomer and dimer, but these might be considered close enough to 2.0 in view of the uncertainties in determining the displacements of a large number of individually weak modes.

More careful examination of the data, however, reveals some inconsistencies with this simple picture. The first is apparent from examination of the absorption spectra alone. Simple

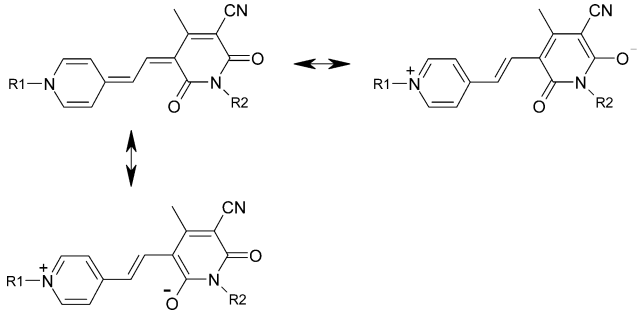

Figure 11. Resonance structures for merocyanine dyes.

exciton-coupling theory predicts that the total oscillator strength of the electronic transition should be conserved upon dimer formation, but in fact the integrated absorptivity on a per chromophore basis is lower for the dimer than for the monomer (see Figure 1 of ref 27). This is also reflected in the fitting parameters of Table 2. The electronic transition dipole length for the dimer is expected to be $\sqrt{2}$ times that of the monomer (the oscillator strength is proportional to $|\mu_{ge}|^2$), but the ratio of dimer-to-monomer transition lengths from Table 2 ranges from 1.24 to 1.31 among the three chromophores, corresponding to oscillator strength ratios between 1.54 and 1.72. (Our simulations with the exponential dephasing model slightly overestimate the oscillator strength of the monomer because of the unphysical exponential tail, but the dimer-to-monomer oscillator strength ratios are clearly smaller than 2.0.) The ZINDO calculations are in qualitative agreement with this observation, giving dimer-to-monomer oscillator strength ratios for the lowest allowed transitions that range from 1.9 to 1.3 as the interplane separation is reduced from 4.0 Å to 3.5 Å. A second inconsistency is apparent from examination of the mode-specific reorganization energies or displacements. Although the change in total vibrational reorganization energy between monomer and dimer is fairly close to what we expect, it is not equally partitioned among the different vibrations as the simple model would predict. Table 2 shows that the higher-frequency modes have their Δ values reduced by less than $\sqrt{2}$ upon dimerization, whereas the lower-frequency modes change by more than $\sqrt{2}$.

There are also some more specific perturbations to the vibrational intensities. As noted above, a few Raman lines of the monomers, particularly the fairly strong ones at 1036 and 1496 cm^{-1}, are essentially undetectable in the dimers. Both of these vibrations appear in the IR spectra with considerable intensity in the samples prepared from both CH_2Cl_2 and dioxane, indicating that their ground-state frequencies are not significantly perturbed by aggregation. This observation seems to rule out a ground-state mechanism, for example, coupling between the vibrational transition dipoles on the two monomers to form symmetric and antisymmetric combinations. Therefore, the disappearance of these two frequencies from the dimer resonance Raman spectra must result from an effect on the excited-state geometries of the dimers. These merocyanine dyes have large dipole moments in both the ground and excited states[27] indicating significant contributions to the structures from resonance forms such as those shown in Figure 11. Some dependence of both vibrational frequencies and resonance Raman intensities on the local environment is thus to be expected. We do not have the definite vibrational assignments that would allow us to fully interpret these dimerization-induced changes, and the mode descriptions given in Table 4 must be considered very tentative. In making these assignments we have preserved the calculated frequency ordering and required that strong Raman lines be assigned to in-plane, relatively symmetric

motions. We have also made use of vibrational spectra and normal mode analyses of related molecules, particularly those containing the *N*-alkylpyridinium moiety.[35−38] The 1496 cm^{-1} line is assigned to a normal mode calculated at 1547 cm^{-1} which involves stretching of the C_e-donor ring bond and of the N−C and N−alkyl bonds in the donor ring. The 1036 cm^{-1} line is assigned as the "trigonal" deformation of the donor pyridinium ring. There is no obvious reason the resonance Raman intensities of these vibrations should be particularly sensitive to dimerization, and further work is needed to interpret these changes.

Our experimental and computational results imply that the spectroscopy of these merocyanine dimers is not adequately described by a simple excitonic-coupling model even though the blue-shift of the allowed absorption and the reduced electron−phonon coupling are qualitatively in agreement with the predictions of that model. At these intermonomer separations the coupling is evidently strong enough that overlap between the orbitals on different monomers and/or electron exchange between monomers make important contributions to the spectroscopy. Vibronic coupling between the higher-energy allowed and lower-energy forbidden transitions of the dimer is also a possibility, although this mechanism would be expected to induce intensity in some Raman transitions that are silent in the monomer, whereas the converse is observed in this system. There are many other systems in which the qualitative predictions of the excitonic-coupling model are borne out despite the clear inadequacy of that model. As perhaps extreme examples, from a purely π-electron point of view 1,3-butadiene might be considered as a J-dimer of ethylene monomers or 1,3,5,7-octatetraene as a J-dimer of butadienes. In each case the "dimer" has a red-shifted absorption relative to the monomer, a greater oscillator strength, and weaker electron−phonon coupling. However, simple quantum chemical calculations show that the π-orbital overlap between "monomers" is nearly as large as that within a single monomer, and the assumptions of the dimer model are not reasonable.

Resonance Raman spectra of covalent and noncovalent homodimers and larger aggregates of several other π-conjugated organic molecules have been reported and analyzed qualitatively.[19,39−46] Akins and co-workers report significant differences in the resonance Raman frequencies and intensities between monomeric, crystalline, and J-aggregated cyanine dyes, but these observations may also be complicated by changes in protonation state.[40−44] Noncovalent[46] and covalent porphyrin aggregates[19] also show some large effects on the vibrational frequencies and Raman intensities. Chen et al.[47] measured and modeled the absorption spectra and Raman excitation profiles of a porphyrin diacid in both monomeric and noncovalent aggregated forms. The strong Soret transition of the monomer is split into both a red-shifted and a blue-shifted band in the aggregate, but it is not clear whether a single type of aggregate produces both bands. The vibrational frequencies and relative intensities in the monomer and both aggregates are generally similar although not identical. The authors modeled the monomer, J-aggregate, and H-aggregate bands as three distinct transitions having independently adjustable modeling parameters and found comparable vibrational displacements in all three bands, with no significant reduction in vibrational reorganization energy in the aggregates. However, they did not measure absolute Raman cross sections and their Raman spectra were obtained at only one (for the H-band) or two (for the J-band) excitation wavelengths, and these data probably did not provide strong constraints on the fitting parameters. In our recent study of cresyl violet dimers on SiO_2,[26] the excitonically coupled homodimer model with the parameters obtained from modeling the monomer gave reasonably good fits to the dimer absorption spectrum and Raman profiles, but both the homogeneous and inhomogeneous widths had to be increased considerably in the dimer, and a few vibrations were clearly anomalous. Straightforward comparison of monomer and dimer in that system is complicated by the additional effects of binding to the SiO_2 surface and possible changes in protonation state upon binding. The merocyanine dyes studied in the current work allow a much cleaner investigation of the effects of dimerization alone.

The spectral simulations that treat the dimer as transition-dipole-coupled monomers are computationally quite difficult owing to the need to perform the calculations in the frequency domain.[11] We cannot directly handle the several dozen Franck−Condon active vibrations present in most large molecules and instead have to use the approximate method of grouping all of the vibrations except the one whose Raman profile is being calculated into a few effective modes.[26] Figure 9 shows that this approximate method gives essentially identical spectra to those calculated for a "supermolecule" having a single allowed electronic transition with vibrational displacements reduced by $\sqrt{2}$. This result shows that our approximation to the explicit dimer calculations is quite accurate. More importantly, it also shows that when the electronic coupling is as strong as it is in these dimers, it is not necessary to treat the dimer as coupled monomers; the dimer can be modeled through our usual, computationally efficient time-dependent formalism as a single electronic transition linearly coupled to harmonic vibrational modes. Sample calculations on a three-mode merocyanine model indicate that the single-transition supermolecule approach is accurate as long as the effective electronic coupling (defined here as twice the separation between the maxima of the two absorption bands, if they both carry oscillator strength) exceeds about 1000 cm^{-1}. This result agrees with previous definitions of the "strong-coupling" limit as that where the splitting between the two electronic transitions is greater than the vibronic bandwidth of each transition.[1] Whether the excitonic-coupling model can be valid when the coupling is this strong remains an open question.

If an excitonic-coupling model is assumed, the effective coupling can be determined by direct inspection of the absorption spectrum in geometries where both the J-band and the H-band have intensity. When only one of the transitions carries intensity, it is tempting to equate the coupling to the blue-shift (for H-dimers) or red-shift (for J-dimers) of the dimer absorption relative to that of the monomer. This assumption, however, neglects the pure "solvent" effect of dimerization on the absorption maximum. When the ground-state dipole moment is large and the change in dipole moment upon excitation is also substantial, as it is with these merocyanines, increasing the solvent polarity generates a large blue-shift in the monomer's absorption maximum (2500 cm^{-1} from dioxane to methanol for PDOP-n). Because a merocyanine molecule is more polar than a weakly polar solvent such as dioxane, dimerization places each monomer in a more polar environment and should blue-shift its absorption spectrum apart from any coupling to the electronic transition of the other monomer. For example, the molecule that differs from PDOP-d only in having a hexyl group rather than butyl on the donor ring exhibits an absorption maximum of 568 nm in the monomer, whereas the dimer shows both a strong H-band at 492 nm and a weakly allowed J-band at 597 nm.[27] The midpoint between the two dimer maxima is 930 cm^{-1} to the blue of the monomer maximum. The coupling strength inferred from the blue-shift of the H-band relative to the

monomer absorption is 2700 cm^{-1}, but this overestimates the true coupling which is better estimated as half the splitting between the H-band and J-band absorptions, or 1800 cm^{-1}.

The center-to-center distances that best reproduce the spectral shifts within the transition-dipole-coupled monomer model (Table 3, about 4.7 Å) are somewhat larger than the intermolecular separations obtained from AM1 energy minimizations. Note that in our definition, the distance R_{ab} is measured between the centers of the two dipoles, $R_{ab} = d/\sin\theta$, where d is the separation between the two molecular planes and θ is the slip angle; at $\theta = 60°$, $R_{ab} = 4.7$ Å corresponds to an interplane separation of 4.07 Å, whereas the AM1 calculations give an interplane separation of about 3.5 Å. The point−dipole approximation used throughout this work should be good only when the intermonomer separation is large compared with the size of each monomer, which is clearly not the case here (refer to the structure in Figure 3). The interacting charge distributions could be treated more accurately by adopting an extended dipole model,[48,49] an expansion including higher multipoles,[50] a multicentric monopole expansion of the transition density,[9,49] or, better yet, a treatment that considers the full spatial distribution of the transition density.[51] Our analysis, however, does not rely upon the validity of the point−dipole approximation because we are not attempting to calculate the strength of the coupling from first principles. The intermonomer separation is treated as an empirical parameter chosen to reproduce the experimental absorption maximum of the H-dimer. The modifications mentioned above would change the intermonomer separation that must be assumed to produce a given coupling strength, but the basic physical description obtained from the excitonically coupled monomer model would not be affected, nor would our conclusions about its validity.

Our results might seem to be at odds with the recent computational work of Beljonne et al., who compared the exciton model with the supermolecule approach for calculating the splitting of the lowest allowed electronic transition of interacting linear polyene chains.[9] They found that the excitonically coupled monomer model gave good agreement with the supermolecule approach as long as atomic transition densities were used instead of the more approximate point−dipole model to calculate the coupling strength. That group, however, performed the majority of their calculations at relatively large intermonomer spacings of 4.5 Å or greater. They comment that the two predictions begin to diverge by the time the separation is reduced to 4 Å or less, indicating contributions from charge-transfer type excitations. Our ZINDO calculations predict significant breakdown of the excitonically coupled monomer picture only for interplane separations of about 4 Å or less, which appears to be the regime in which our merocyanine dimers fall.

6. Conclusions

The basic features of the optical absorption spectra and resonance Raman excitation profiles of these merocyanine H-dimers are reasonably well explained by the simple molecular exciton model which assumes that the two monomers interact through coupling between their transition dipole moments. The allowed electronic transition is strongly blue-shifted as expected for a stacked antiparallel dimer, and quantitative simulation of the resonance Raman excitation profiles indicates generally reduced coupling of the electronic transition to molecular vibrations, consistent with delocalization of the excitation over both chromophores. Most of the vibrational frequencies are affected weakly if at all by dimerization. However, some vibrations suffer large intensity perturbations, indicating specific effects of dimerization on the geometric distortions caused by electronic excitation. These experimental data, combined with the results of semiempirical quantum chemical calculations on the dimers, lead us to conclude that the excitonically coupled monomer model is not adequate to describe the spectroscopy of these noncovalent dimers. A supermolecule picture that treats the dimer as a new molecule is required to correctly describe the electronic excitations of these strongly interacting dimers.

Acknowledgment. This work was supported by NSF Grants No. CHE-0109920 to Kansas State University and No. CHE-0342816 to the University of California, Merced, and by Grant No. N00014-02-1-0584 from the Office of Naval Research to Kansas State University.

References and Notes

(1) Fulton, R. L.; Gouterman, M. *J. Chem. Phys.* **1964**, *41*, 2280−2286.
(2) Kasha, M.; Rawls, H. R.; El-Bayoumi, M. A. *Pure Appl. Chem.* **1965**, *11*, 371−392.
(3) Philpott, M. R. *Adv. Chem. Phys.* **1973**, *23*, 227−341.
(4) Gregory, A. R.; Henneker, W. H.; Siebrand, W.; Zgierski, M. Z. *J. Chem. Phys.* **1975**, *63*, 5475−5489.
(5) Friesner, R.; Silbey, R. *J. Chem. Phys.* **1981**, *75*, 5630−5639.
(6) Spano, F. C. *J. Chem. Phys.* **2001**, *114*, 5376−5390.
(7) Renge, I.; Wild, U. P. *J. Phys. Chem. A* **1997**, *101*, 7977−7988.
(8) Freiberg, A.; Timpmann, K.; Ruus, R.; Woodbury, N. W. *J. Phys. Chem. B* **1999**, *103*, 10032−10041.
(9) Beljonne, D.; Cornil, J.; Silbey, R.; Millié, P.; Brédas, J. L. *J. Chem. Phys.* **2000**, *112*, 4749−4758.
(10) Mizuguchi, J.; Tojo, K. *J. Phys. Chem. B* **2002**, *106*, 767−772.
(11) Kelley, A. M. *J. Chem. Phys.* **2003**, *119*, 3320−3331.
(12) Wu, H.-M.; Ratsep, M.; Lee, I.-J.; Cogdell, R. J.; Small, G. J. *J. Phys. Chem. B* **1997**, *101*, 7654−7663.
(13) Bazan, G. C.; Oldham, W. J., Jr.; Lachicotte, R. J.; Tretiak, S.; Chernyak, V.; Mukamel, S. *J. Am. Chem. Soc.* **1998**, *120*, 9188−9204.
(14) Oldham, W. J., Jr.; Miao, Y.-J.; Lachicotte, R. J.; Bazan, G. C. *J. Am. Chem. Soc.* **1998**, *120*, 419−420.
(15) Wang, S.; Bazan, G. C.; Tretiak, S.; Mukamel, S. *J. Am. Chem. Soc.* **2000**, *122*, 1289−1297.
(16) Zyss, J.; Ledoux, I.; Volkov, S.; Chernyak, V.; Mukamel, S.; Bartholomew, G. P.; Bazan, G. C. *J. Am. Chem Soc.* **2000**, *122*, 11956−11962.
(17) Verdal, N.; Godbout, J. T.; Perkins, T. L.; Bartholomew, G. P.; Bazan, G. C.; Kelley, A. M. *Chem. Phys. Lett.* **2000**, *320*, 95−103.
(18) Moran, A. M.; Bartholomew, G. P.; Bazan, G. C.; Kelley, A. M. *J. Phys. Chem. A* **2002**, *106*, 4928−4937.
(19) Bhuiyan, A. A.; Seth, J.; Yoshida, N.; Osuka, A.; Bocian, D. F. *J. Phys. Chem. B* **2000**, *104*, 10757−10764.
(20) Jeong, D. H.; Yoon, M.-C.; Jang, S. M.; Kim, D.; Cho, D. W.; Yoshida, N.; Aratani, N.; Osuka, A. *J. Phys. Chem. A* **2002**, *106*, 2359−2368.
(21) Jeong, D. H.; Jang, S. M.; Hwang, I.-W.; Kim, D.; Matsuzaki, Y.; Tanaka, K.; Tsuda, A.; Nakamura, T.; Osuka, A. *J. Chem. Phys.* **2003**, *119*, 5237−5252.
(22) Fletcher, J. T.; Therien, M. J. *J. Am. Chem. Soc.* **2002**, *124*, 4298−4311.
(23) Kumble, R.; Palese, S.; Lin, V. S.-Y.; Therien, M. J.; Hochstrasser, R. M. *J. Am. Chem. Soc.* **1998**, *120*, 11489−11498.
(24) Martini, I.; Hartland, G. V.; Kamat, P. V. *J. Phys. Chem. B* **1997**, *101*, 4826−4830.
(25) Liu, D.; Kamat, P. V. *J. Chem. Phys.* **1996**, *105*, 965−970.
(26) Leng, W.; Kelley, A. M. *Langmuir* **2003**, *19*, 7049−7055.
(27) Würthner, F.; Yao, S.; Debaerdemaeker, T.; Wortmann, R. *J. Am. Chem. Soc.* **2002**, *124*, 9431−9447.
(28) Reference 27 gives error estimates of ±0.2 kJ $mole^{-1}$ in the free energy of dimerization, which translates to an uncertainty in dimer concentration of only about 1% within our experimental concentration range. Additional sources of concentration error in our Raman experiments arise from small fluctuations in the ambient temperature and slight evaporation of the highly volatile solvent. We estimate dimer concentration uncertainties of about ±5% in our experiments.
(29) Myers, A. B. In *Laser Techniques in Chemistry*; Myers, A. B., Rizzo, T. R., Eds.; Wiley: New York, 1995; pp 325−384.
(30) The mixed Gaussian−Lorentzian line shape is a flexible function that allows all of the spectra to be fit in a consistent manner, although this function has no solid theoretical basis. The adequacy of the fits was judged

by not only the rms fitting error but also the consistency of the peak frequencies and widths from one excitation wavelength to another. Typically, the frequencies were constant to within the calibration uncertainty ($\sim$1 cm^{-1}) and the widths were constant to within $\sim$1.5 cm^{-1}.

(31) Moran, A. M.; Delbecque, C.; Kelley, A. M. *J. Phys. Chem. A* **2001**, *105*, 10208−10219.

(32) Myers, A. B. *J. Raman Spectrosc.* **1997**, *28*, 389−401.

(33) Frisch, M. J.; Trucks, G. W.; Schlegel, H. B.; Scuseria, G. E.; Robb, M. A.; Cheeseman, J. R.; Zakrzewski, V. G.; Montgomery, J. A., Jr.; Stratmann, R. E.; Burant, J. C.; Dapprich, S.; Millam, J. M.; Daniels, A. D.; Kudin, K. N.; Strain, M. C.; Farkas, O.; Tomasi, J.; Barone, V.; Cossi, M.; Cammi, R.; Mennucci, B.; Pomelli, C.; Adamo, C.; Clifford, S.; Ochterski, J.; Petersson, G. A.; Ayala, P. Y.; Cui, Q.; Morokuma, K.; Malick, D. K.; Rabuck, A. D.; Raghavachari, K.; Foresman, J. B.; Cioslowski, J.; Ortiz, J. V.; Stefanov, B. B.; Liu, G.; Liashenko, A.; Piskorz, P.; Komaromi, I.; Gomperts, R.; Martin, R. L.; Fox, D. J.; Keith, T.; Al-Laham, M. A.; Peng, C. Y.; Nanayakkara, A.; Gonzalez, C.; Challacombe, M.; Gill, P. M. W.; Johnson, B. G.; Chen, W.; Wong, M. W.; Andres, J. L.; Head-Gordon, M.; Replogle, E. S.; Pople, J. A. *Gaussian 98*, revision A.7; Gaussian, Inc.: Pittsburgh, PA, 1998.

(34) Li, B.; Johnson, A. E.; Mukamel, S.; Myers, A. B. *J. Am. Chem. Soc* **1994**, *116*, 11039−11047.

(35) Hester, R. E.; Suzuki, S. *J. Phys. Chem.* **1982**, *86*, 4626−4630.

(36) Tsukada, M.; Mineo, Y.; Itoh, K. *J. Phys. Chem.* **1989**, *93*, 7989−7992.

(37) Mineo, Y.; Itoh, K. *J. Phys. Chem.* **1991**, *95*, 2451−2456.

(38) Cao, X.; McHale, J. L. *J. Chem. Phys.* **1998**, *109*, 1901−1911.

(39) Hochstrasser, R. M.; Nyi, C. A. *J. Chem. Phys.* **1980**, *72*, 2591−2600.

(40) Akins, D. L.; Macklin, J. W.; Zhu, H. R. *J. Phys. Chem.* **1991**, *95*, 793−798.

(41) Akins, D. L.; Macklin, J. W. *J. Phys. Chem.* **1989**, *93*, 5999−6007.

(42) Akins, D. L.; Zhuang, Y. H.; Zhu, H.-R.; Liu, J. Q. *J. Phys. Chem.* **1994**, *98*, 1068−1072.

(43) Akins, D. L.; Özcelik, S.; Zhu, H.-R.; Guo, C. *J. Phys. Chem. A* **1997**, *101*, 3251−3259.

(44) Guo, C.; Aydin, M.; Zhu, H.-R.; Akins, D. L. *J. Phys. Chem. B* **2002**, *106*, 5447−5454.

(45) Okamoto, H.; Hamaguchi, H.; Tasumi, M. *J. Raman Spectrosc.* **1989**, *20*, 751−756.

(46) Diers, J. R.; Zhu, Y.; Blankenship, R. E.; Bocian, D. F. *J. Phys. Chem.* **1996**, *100*, 8573−8579.

(47) Chen, D.-M.; He, T.; Cong, D.-F.; Zhang, Y.-H.; Liu, F.-C. *J. Phys. Chem. A* **2001**, *105*, 3981−3988.

(48) Czikklely, V.; Forsterling, H. D.; Kuhn, H. *Chem. Phys. Lett.* **1970**, *6*, 207−210.

(49) Marguet, S.; Markovitsi, D.; Millié, P.; Sigal, H.; Kumar, S. *J. Phys. Chem. B* **1998**, *102*, 4697−4710.

(50) Stone, A. J. *The Theory of Intermolecular Forces*; Oxford University Press: New York, 1996.

(51) Krueger, B. P.; Scholes, G. D.; Fleming, G. R. *J. Phys. Chem. B* **1998**, *102*, 5378−5386.